Chapter 19

High-temperature polybenzimidazole-based membranes

D. C. Seel[1], B. C. Benicewicz[1], L. Xiao[2] and T. J. Schmidt[3]

[1] *University of South Carolina, Columbia, SC, USA*
[2] *BASF Fuel Cell Inc., Somerset, NJ, USA*
[3] *BASF Fuel Cell GmbH, Frankfurt am Main, Germany*

1 INTRODUCTION

Polybenzimidazole (PBI)-based high-temperature proton exchange membranes (PEMs) offer many advantages that aid in a simplified fuel cell system design. Such benefits include high resistance to fuel impurities (most notably carbon monoxide), fast electrode kinetics, and simplified water and thermal management due to operational temperatures above 120 °C.[1] As a result of its intrinsic physicochemical properties, e.g., heat resistance and proton conductivity above 100 °C without humidification, PBI has emerged as a prime candidate for low-cost PEMs (see **High-temperature membranes**, Volume 3).[2] Additionally, several PBI chemistries prepared through the polyphosphoric acid (PPA) process have been shown to possess improved characteristics and have overcome some of the limiting factors associated with conventionally prepared PBI membranes imbibed with phosphoric acid (PA) electrolyte.[3, 4]

2 POLYBENZIMIDAZOLE SYNTHESIS

PBIs are produced through the step-growth polymerization (Scheme 1) of a tetraamine, e.g., 3,3′,4,4′-tetraaminobiphenyl (TAB), and a dicarboxylic acid or a diacid derivative, to yield heterocyclic polymers that display high proton conductivity up to 200 °C when appropriately doped with strong acids; such behavior at high temperature eliminates the need for water as a solvating agent and a proton transport medium, commonly required in other membrane materials.

2.1 Conventional PBI membrane synthesis

The conventional method to prepare PA-doped PBI membranes is a multistep procedure that involves the dissolution and casting of commercially available PBI from a suitable organic solvent such as *N,N*-dimethylacetamide (DMAc) with lithium chloride as a stabilizing agent (see **High-temperature membranes**, Volume 3). The film produced after casting is imbibed by soaking in a PA bath for several hours[5–7] and yields PBI membranes with low PA loadings (generally 5–16 mol of PA per mole PBI repeat unit).[5, 8, 9]

In general, PBI membranes with higher PA-doping levels produce membranes with higher proton conductivity membranes. PBI membranes prepared from the conventional imbibing method, however, have been shown to have increasingly poor mechanical properties with increased PA doping and are therefore unsuitable for fuel cell applications.[10]

2.2 The polyphosphoric acid (PPA) process

A new process to produce PBI membranes for fuel cell applications has been developed to overcome the limiting factors of the conventional PBI processing method.

Handbook of Fuel Cells – Fundamentals, Technology and Applications. Edited by Wolf Vielstich, Harumi Yokokawa, Hubert A. Gasteiger. Volume 5: *Advances in Electocatalysis, Materials, Diagnostics and Durability*. ISBN: 978-0-470-72311-1.

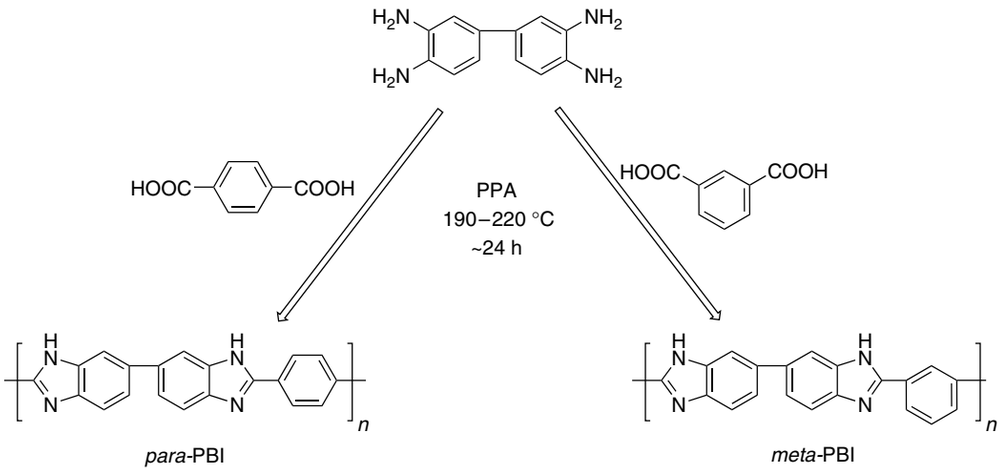

Scheme 1. General synthetic scheme for the synthesis of PBI in PPA (polyphosphoric acid).

This novel process, termed the *PPA process*, produces high molecular weight polymer with a membrane structure capable of attaining high acid-doping levels while maintaining good mechanical properties and excellent long-term stability.

The PPA process utilizes a widely employed polycondensation agent, PPA, to perform as a condensation reagent as well as casting solvent in a single step, one-pot polymerization. The general procedure for the synthesis of PBIs by the PPA process was previously reported by Xiao *et al.*[3] The synthesis is performed by combining a dicarboxylic acid and a tetraamine with PPA in a suitable reaction vessel. The reaction temperature is controlled by a programmable temperature controller and an oil bath during a ramp and soak procedure. Typical polymerization temperatures are approximately 190–220 °C for 16–24 h.[3] Under the appropriate reaction conditions, high molecular weight PBI polymer is produced. Polymer solutions of PBI in PPA are directly cast into films and upon exposure to ambient moisture, PPA is hydrolyzed to PA to yield highly PA-doped PBI membranes. A transition from the polymer solution state to a gel state is observed during the hydrolysis as PPA (a good solvent for PBI) is converted *in situ* to PA (a poor solvent for PBI). This sol–gel transition results in a mechanically stable, highly conductive PEM that is capable of operating at high temperature without humidification of feed gases. The multiple chemical reactions and physical transitions that occur during the PPA process have been summarized in a "state diagram", as shown in Figure 1.[3] The details of the phase diagram and the sol–gel transition illustrated in Figure 1 change with different polymer structures and processing conditions. However, many polymer chemical structures provide excellent gel stability up to 200 °C. Furthermore, the stability of the gel phases is also aided by the difficulty in thermally converting PA to PPA at this temperature range.

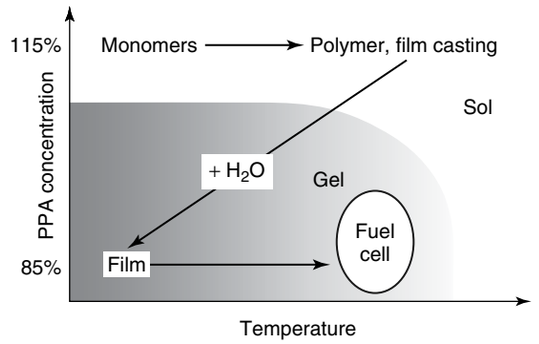

Figure 1. State diagram of the PPA sol–gel preparation process.

The induced sol–gel transition unique to the PPA process is vital in the preparation of PBI membranes that exhibit substantially different properties than the conventionally imbibed membranes. Greenbaum *et al.*[4] employed nuclear magnetic resonance (NMR) to explore the differences in transport properties between conventionally imbibed PBI and PBI prepared by the PPA process. The PBI samples prepared by the PPA process and the conventional method differed only in membrane preparation, but were similar in polymer weight percent, PA loading, and water content. Although different inherent viscosities (IV), or relative measures of molecular weight, are seen for each polymer as a result of the different polymer processing methods, both preparation methods are effective in producing doped PBI membranes. As seen in Table 1, the proton diffusion coefficient and bulk conductivity of the PPA-prepared *meta*-polybenzimidazole (*m*-PBI) membrane were significantly higher than the conventionally imbibed membrane.

Owing to the discrepancy in proton conductivities of two identical chemistries prepared by different methods, it can be concluded that the PPA process imparts a polymer membrane structure capable of providing a proton transport mechanism that is more efficient than that of the

Table 1. Comparison of H_3PO_4 *m*-PBI membranes prepared by different methods.

IV[a] (dl g^{-1})	Film process	Polymer (wt%)	PA (wt%)	Water (wt%)	PA/PBI (molar ratio)	Proton diffusion coefficient[b] ($cm^2\ s^{-1}$)	Conductivity[c] ($S\ cm^{-1}$)
0.89	Conventionally imbibed	15.6	60.7	23.7	12.2	10^{-7}	0.048
1.49	PPA process	14.4	63.3	22.3	13.8	3×10^{-6}	0.13

[a] Inherent viscosity (IV) was measured at a polymer concentration of $0.2\ g\ dl^{-1}$ in concentrated sulfuric acid (96%) at 30 °C, using a Canon Ubbelohde viscometer
[b] Estimation of upper bound for conventionally imbibed *m*-PBI at 180 °C; PPA-prepared *m*-PBI measured at 180 °C
[c] Measured at 160 °C after an initial heating to 160 °C to remove water

conventional membrane. The work of Greenbaum *et al.* supported this conclusion through extensive proton (^1H) and phosphorous (^{31}P) NMR.[4]

2.3 PBI chemistries prepared through the PPA process

Several PBI chemistries prepared through the PPA process have been explored, including AB-PBI, *meta*-polybenzimidazole (*m*-PBI), *para*-polybenzimidazole (*p*-PBI), pyridine-based PBIs, and sulfo-PBIs.[3, 11, 12] Most work thus far has focused on *m*- and *p*-PBI and is the major focus of discussion in this article.

The mechanical and PEM characteristics of PBI are very much dependent on the polymer's chemical structure. One of the primary effects of the polymer's chemical structure is the amount of PA retained in the membrane, ranging from 3 to >50 mol of PA per mol of polymer repeat unit for different PBI chemistries (e.g., ratios of 12.2 and 13.8 for the materials shown in Table 1). Also, some of the more soluble PBIs remain in solution after the hydrolysis procedure and are too soluble to form films. Ongoing research has continued to explore additional PBI chemistries with the end goal of improving PEM characteristics.

2.4 The physical and chemical properties of PBI

m-PBI was the first PEM to be developed by the PPA process. The membrane showed proton conductivities as high as $0.13\ S\ cm^{-1}$ at 160 °C (see Table 1) and good mechanical properties with PA loadings of 14–26 mol of PA per mole of PBI repeat unit. At PA loading levels of 25 mol of PA per mole of polymer repeat unit, typical room temperature tensile strength and elongation at break values for *m*-PBI are 1.6 MPa and 250%, respectively.

Compared to *m*-PBI, the PA loadings and proton conductivities of *p*-PBI were reported to be higher in films that retained mechanical stability.[3] Typical PA loadings of *p*-PBI membranes ranged from 20 to 40 mol of PA per mol PBI repeat unit and conductivities of $0.01\ S\ cm^{-1}$ at room temperature up to $0.26\ S\ cm^{-1}$ at 200 °C. The mechanical properties of the stiffer-chained *p*-PBI showed improvement over that of *m*-PBI as well, having similar mechanical properties at higher PA-doping levels. A typical tensile strength value for *p*-PBI is 1.7 MPa at an acid-doping level

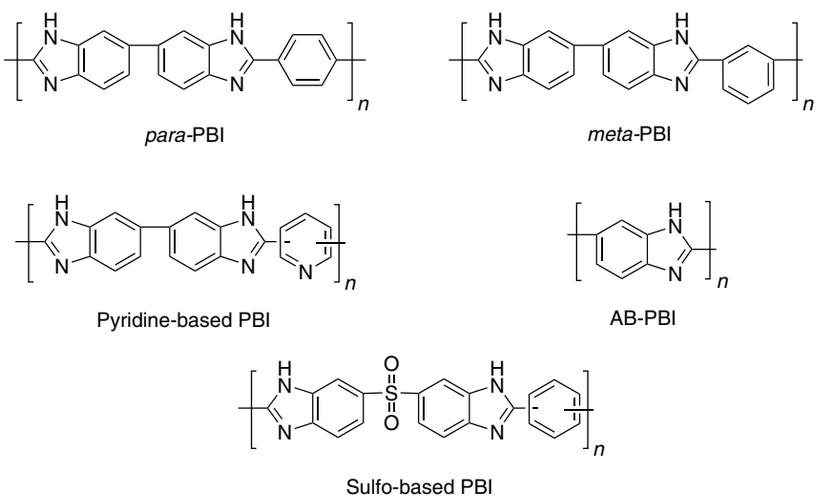

Scheme 2. Examples of polybenzimidazole (PBI) chemistries prepared through the polyphosphoric acid (PPA) process.

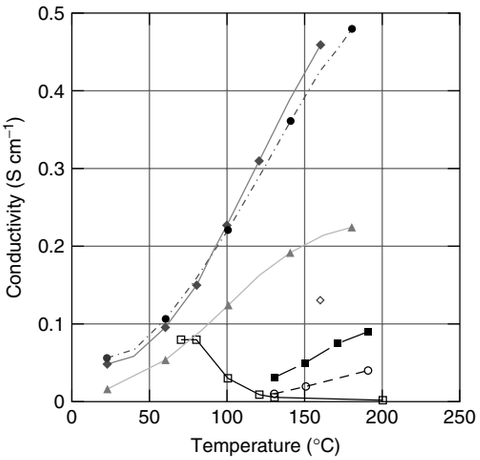

Figure 2. Through-plane conductivity–temperature behavior for several PEMs (□ Nafion, ■ PBI cast from trifluoroacetic acid, ◊ *m*-PBI cast from DMAc (conventional membrane preparation),[9] ○ PBI from conventional DMAc casting method, ● ♦ ▲ *p*-PBI chemistries prepared via the PPA process). All membranes were prepared in the Benicewicz research group at Rensselaer Polytechnic Institute. [Reproduced from Ref. [9] © Springer, 2001.]

of 36 mol of PA per mol of PBI repeat unit.[3] Figure 2 shows the conductivity–temperature behavior for several different proton exchange membranes.

2.5 Other proton conductors for use in high-temperature fuel cells

2.5.1 SiC matrix used in phosphoric acid fuel cells

In order to use PA as the electrolyte in commercial PA fuel cell stacks, the acid has to be embedded into a matrix material, which can withstand both the acidic environment and the operation temperature. In 1970, it was discovered that SiC was the material of choice.[13] Initially, approximately 5-μm SiC particles and 5 wt% polytetrafluoroethylene (PTFE) were sprayed onto the electrodes and heat treated at 310 °C in order to bond the structure together and form a relatively self-standing matrix. At lower particle sizes implemented later (approximately 1 μm), matrices could also be formed without using a PTFE binder (see **Stack materials and stack design**, Volume 4). In order to keep the resistance low, the thickness of the matrix was approximately 50–100 μm[14, 15] with effective ionic conductivities of approximately 0.05–0.15 S cm^{-1} at operating conditions of 180–200 °C. However, to guarantee long life in the fuel cell stack, it had to be ensured that the porosity of approximately 50% was maintained and that the pore-size distribution (concomitant with the respective bubble pressure of 70 kPa or greater) of the SiC matrix did not change much during stack life since the interaction of matrix and PA was only of a physical nature. That is, the acid was held in place solely by capillary forces of the pores in the matrix. If the bubble pressure became too low during operation, the acid could be easily removed from the matrix. However, SiC electrolyte matrices were used in the commercial PC 25 phosphoric acid fuel cell (PAFC) power plants from UTC and allowed stack operation for 40 000 h or more (see **Experience with 200 kW PC25 fuel cell power plant**, Volume 4).

2.5.2 Solid acid separators

Solid inorganic proton conductors like $CsHSO_4$ or CsH_2PO_4 were first used as separators in fuel cells by Haile and coworkers[16, 17] in so-called solid acid fuel cells, although this group of materials has been known for a long time as solid proton conductors, e.g., solid acidic sulfates, phosphates, or selenates.[18] Generally, at room temperature, these materials are low-symmetry solids with low proton conductivity and well-ordered hydrogen bonds between, e.g., well-ordered HSO_4^- tetrahedra. Upon increasing the temperature above certain limit (approximately 140 °C for $CsHSO_4$ and 230 °C for CsH_2PO_4), these solid acids undergo a phase transition into a highly symmetric so-called plastic phase with high proton conductivity. The plastic phase can be described as a phase with long range order but local dynamic reorientational disorder of the sulfate tetrahedra[18] and thought of as a solid with some liquidlike properties.[18] In $CsHSO_4$, the increased proton conductivity can be ascribed to fast hydrogen bond breaking and diffusion concomitant with fast reorientation of the sulfate tetrahedra. Similar to pure PA, where only the proton is diffusing while the $H_2PO_4^-$ maintain their positions, in $CsHSO_4$, the sulfates maintain their position in the crystals. Uda and Haile also demonstrated the feasibility of using CsH_2PO_4 as proton conductor in single-cell measurements at 240 °C with peak power densities of up to 0.415 W cm^{-2} at approximately 0.35 V using humidified hydrogen and oxygen.[17] At 0.6 V, approximately 0.3 W cm^{-2} could be demonstrated with a separator thickness of 25 μm. However, to reach these single-cell performances, Pt loadings of up to 15 mg cm^{-2} were used. Nevertheless, these lab cell experiments show some potential for using solid acids as separators in fuel cells.

3 COMMERCIAL SOURCES OF PBI MEAS

PBI prepared through the PPA process is commercially available from BASF Fuel Cell (formerly PEMEAS) in the form of membrane electrode assemblies (MEAs). Three generations of PBI MEAs have been developed by BASF Fuel Cell using a state-of-the-art manufacturing line. These MEAs include Celtec® L, Celtec®-P1000, and Celtec® V, a newly designed PBI membrane for use in direct methanol

fuel cells (DMFCs). Currently, the commercial product is the Celtec-P1000 MEA.

3.1 Properties of commercial Celtec®-P1000 MEAs

The Celtec®-P1000 MEA available from BASF Fuel Cell has been shown to have a long lifetime and a high tolerance to typical reformate impurities such as carbon monoxide (CO) and hydrogen sulfide (H_2S). The typical performance properties of Celtec-P1000 MEAs are summarized in Figure 3(a) showing $I-E$ curves with pure hydrogen and with a common steam reformate. It becomes clear from Figure 3(a) that even with 2% by volume of CO in the anode stream, the performance can be maintained close to the performance with pure hydrogen. In order

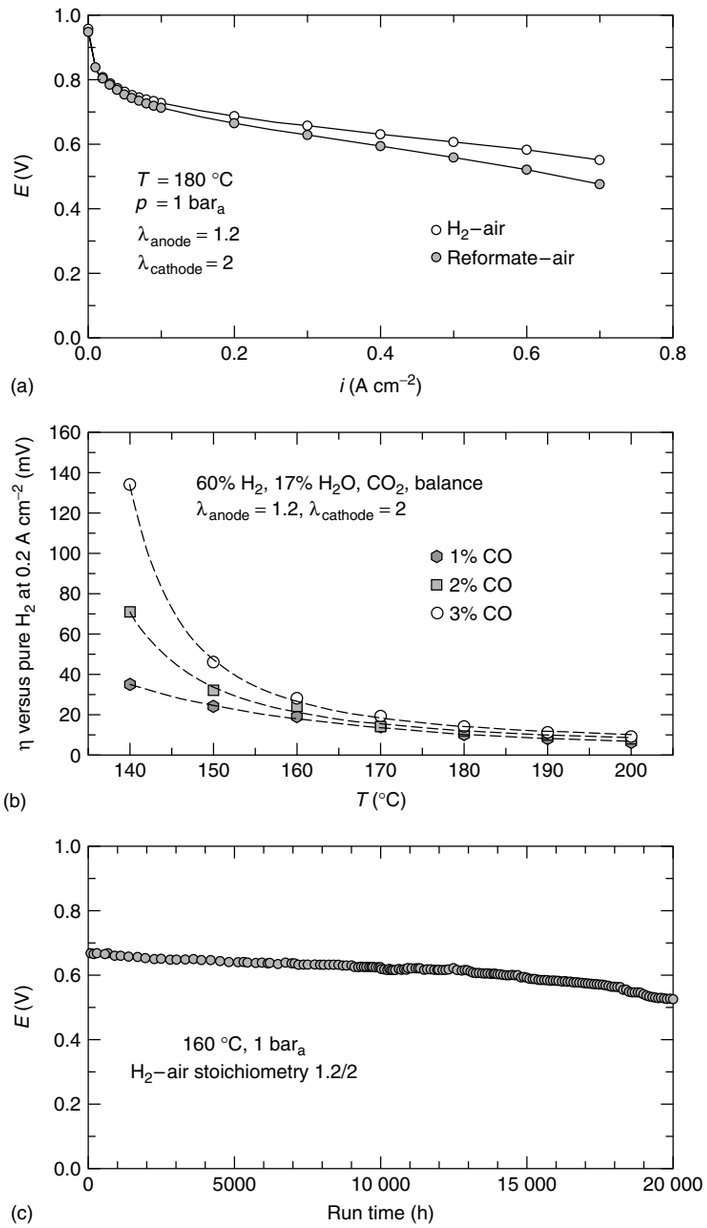

Figure 3. Celtec®-P1000 MEA performance and degradation (single-cell data, 50 cm^2, 1.7 mg cm^{-2} total Pt loading). (a) H_2–air and reformate–air polarization curves at 180 °C, 1 bar_a, stoichiometry 1.2/2, reformate composition 70% H_2, 2% CO, balance CO_2 (nonhumidified gases). (b) Anode overpotential versus pure hydrogen operation as function of temperature and CO partial pressure. Base reformate contains 60% H_2, 17% H_2O, balance CO_2 and the CO concentration as shown in the figure. Anode stoichiometry 1.2, 1 bar_a (anode Pt loading is 1 mg cm^{-2}). (c) Long-term durability test at 160 °C, H_2 air, 1 bar_a, stoichiometry 1.2/2.

to demonstrate, in more detail, the unique CO tolerance of Celtec-P1000 MEAs, Figure 3(b) illustrates the anode overpotentials of different CO containing steam reformates (reformate composition is 60% H_2, 17% H_2O, 1–3% CO, balance CO_2) versus the same reformate without CO contaminant. At a typical stack operation temperature range of 170–180 °C, only small overpotential changes are observed when the CO partial pressure is changed, opening very broad operating windows with respect to operation temperature and anode gas composition. Lifetime tests at steady-state operation and 160 °C, with no humidification, shows a voltage drop of less than $6\,\mu V\,h^{-1}$ and a lifetime of at least 20 000 h (Figure 3c) using pure hydrogen and air at a H_2–air stoichiometry of 1.2/2.0.[19] Finally, MEA testing at 180 °C using wet reformate with 2% CO and 5-ppm H_2S shows an average voltage drop approximately $17\,\mu V\,h^{-1}$ during a 3500-h test, proving a high tolerance to sulfur and no additional anode degradation compared to pure reactants at 180 °C.[20]

3.2 Applications of PBI MEAs

Several applications exist for the PBI fuel cell MEAs, including the use of Celtec®-P1000 MEAs in systems for stationary power needs, e.g., backup power units, combined heat and power (CHP) systems, and microportable power applications, such as small systems for battery replacement. Figure 4 illustrates two real-life examples based on Celtec MEAs, including a 5-kW CHP system for home energy supply and a miniature reformed methanol system (25 W) for use as a battery backup system.[21] Celtec® V applications include stationary and mobile devices based on methanol fuel cells.[22]

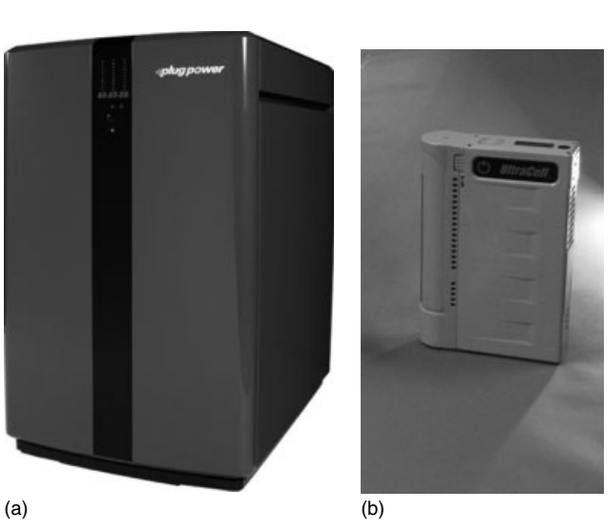

Figure 4. Fuel cell systems based on Celtec MEA technology (a) GenSys® 5-kW high-temperature combined heat and power system from Plug Power. Picture is provided and copyrighted by Plug Power. (b) Ultracell's XX25 25 W high-temperature reformed methanol system sized 15 cm × 23 cm × 4.3 cm weighing 1.24 kg (www.ultracellpower.com). Picture is provided and copyrighted by Ultracell.

More recently, PBI-based membranes prepared through the PPA process have been used for electrochemical hydrogen pumping.[23] An efficient hydrogen purification process was developed that employs the highly proton-conducting PBI membrane to purify reformate streams containing relatively high amounts of carbon monoxide (CO) (approximately 1%) during high-temperature operation under humidified and nonhumidified conditions.[23] This system, therefore, provides a fast and efficient delivery of pure hydrogen from any contaminated hydrogen source while demonstrating excellent CO tolerance.

4 REAL-LIFE CHALLENGES FOR HT PBI-BASED MEAs

After giving general technical information about the chemistry of PBI polymers, membranes, and MEAs, respectively, this part of the article gives more details on real-life operation and challenges of fuel cells operating with PBI-based MEAs. From the scientific and technical perspective, for MEA suppliers, the following question must be considered: how can the performance and lifetime of the MEA be improved with (preferentially) reduced noble metal loading? The driving force here is satisfying the technical and scientific goal to create "better" materials, e.g., more efficient catalysts, more corrosion-stable catalysts, chemically and physically more stable polymers and membranes, or to design "better" interaction of the individual materials used in an MEA, e.g., improving catalyst layer membrane lamination, and proper integration of sealing materials into the MEA. On the other hand, there are processing and commercial aspects, which sometimes may not coincide with the technical aspects. From the commercial point of view, the final fuel cell system application always has to be considered. Further considerations include necessary lifetime in order to make the fuel cell system useful with respect to competing technologies, how significant the size requirements are, as well as others. Some contrast is typically seen with the question of noble metal loadings; scientifically, one would like to reduce the noble metal loading as much as technically possible, but commercially it may not be necessary, especially when recycling plans are in place. In summary, there is one underlying challenge for basically all fuel cell developers independent of commercial or technical perspective, and that is improving durability and performance. The importance of fuel cell durability is clearly recognized and much of the current research and development is related to this topic (see **Proton exchange membrane fuel cell degradation: mechanisms and recent progress**; **Catalyst and catalyst-support durability**; **Highly durable**

PFSA membranes, Volume 5).[19, 20, 24–27] In the following sections, we focus on selected topics related to performance and durability of high-temperature PEMFC MEAs.

4.1 Reducing the cathode overpotential

Although the performance of Celtec P1000 MEAs is high (Figure 3), and basically on the level of typical PAFCs, as compared to typical low-temperature fuel cells, some performance differences can be observed. Since the kinetics for the anode reaction should be similar or even better in the case of high-temperature operation, the main performance difference compared to a low-temperature fuel cell is likely to be found on the cathode. In Figure 5(a), a comparison of the IR-free cathode performances using pure hydrogen and oxygen of a typical low-temperature (LT) MEA at 60 °C and a high-temperature (HT) MEA at 160 °C is plotted. The LT-data are extracted from the work of Neyerlin *et al.*[28] Quite obviously, the slope of the two $i-E$ lines both follow approximately 2.3 RT/F. That is, in both the low- and high-temperature cases, the oxygen kinetics appear to follow Tafel kinetics with slopes of approximately 65 mV/dec and 90 mV/dec (a typical value for Tafel slopes at 160 °C in PA[29]) implying that in both cells the cathodes are running under pure kinetic reaction control (absence of mass-transport overpotentials). It also implies a transfer coefficient, α_c, of unity. In order to

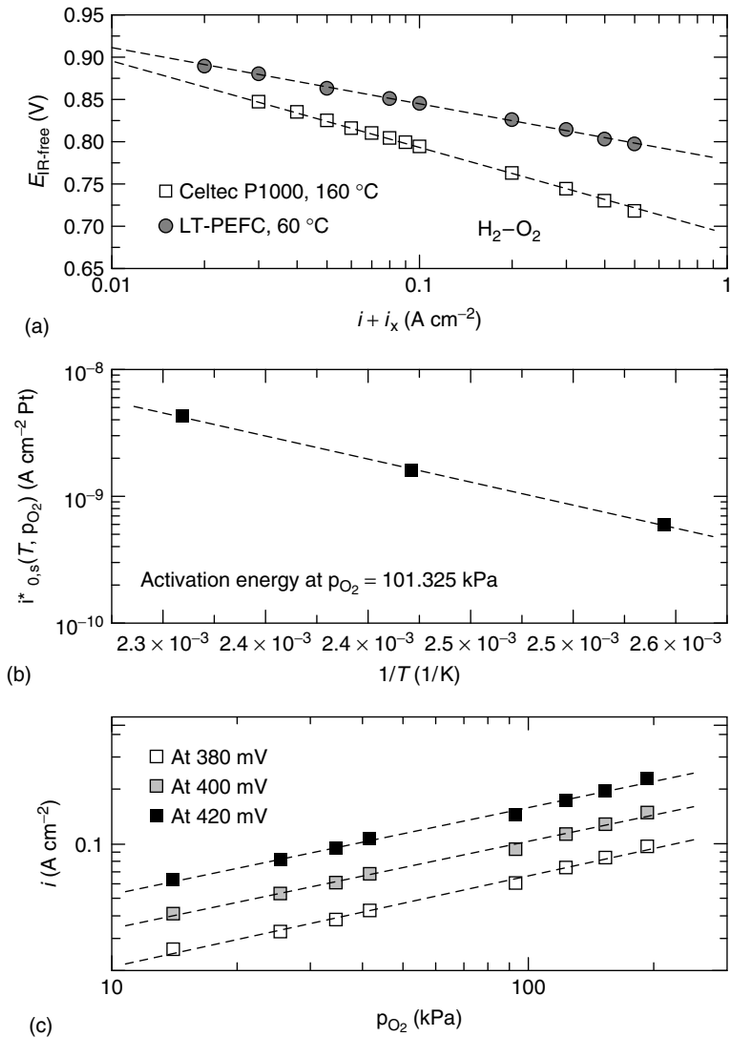

Figure 5. (a) comparison of Tafel plots of HT Celtec P1000 cathode (1 mg cm^{-2}, 160 °C, 100 kPa$_a$, dry H_2/O_2 at $s = 1.2/9.5$) and low-temperature Nafion-type cathode (0.2 mg cm^{-2}, 60 °C, 101 kPa$_a$ H_2 and O_2 partial pressures, 100%RH). Low-temperature data are extracted from Neyerlin *et al.*[28] (b) Plot for determination of activation energy at zero ORR overpotential for the ORR of a Celtec P1000 cathode. (c) Determination of the kinetic reaction order of the ORR using a Celtec P1000 cathode. [Reproduced by permission of ECS – The Electrochemical Society.]

understand the apparent kinetic differences between low- and high-temperature cathodes, it is necessary to determine and compare the kinetic parameters, which are describing the oxygen-reduction reaction (ORR) kinetics, such as the activation energy, the reaction order, and the exchange current density.

Under the applied conditions in Figure 5(a) and the assumption of negligible hydrogen oxidation overpotentials[30] at the elevated temperatures used in this study, the cell performance can be given by equation (1)

$$E_{\text{cell,IR-free}} = E^0(\text{p}_{\text{H}_2/\text{O}_2/\text{H}_2\text{O}}, T) - \eta_{\text{ORR}} \tag{1}$$

where $E_{\text{cell,IR-free}}$, $E^0(\text{p}_{\text{H}_2/\text{O}_2/\text{H}_2\text{O}}, T)$ and η_{ORR} are the IR-corrected cell potential, the partial pressure and temperature-dependent reversible potential, and the overpotential for the ORR, respectively. The equilibrium potential that is dependent on the temperature and partial pressures is calculated according to equation (2)

$$E^0(\text{p}_{\text{H}_2/\text{O}_2/\text{H}_2\text{O}}, T) = E^{0,*} + \frac{\partial E^{0,*}}{\partial T} \cdot (T - 298\ \text{K}) + \left(\frac{2.303RT}{2F}\right) \log\left(\frac{\overline{\text{p}}_{\text{H}_2} \cdot \overline{\text{p}}_{\text{O}_2}{}^{0.5}}{\overline{\text{p}}_{\text{H}_2\text{O}}}\right) \tag{2}$$

where the first term, $E^{0,*}$, is the equilibrium potential at 298 K and 101 325 Pa calculated from ΔG values for gas-phase water[31]; the second term is used to correct $E^{0,*}$ for the temperature, calculated using ΔS values for gas-phase water[31]; the third Nernstian term corrects $E^{0,*}$ for the individual partial pressures. $\overline{\text{p}}_{\text{H}_2}$, $\overline{\text{p}}_{\text{O}_2}$, $\overline{\text{p}}_{\text{H}_2\text{O}}$ are the mean partial pressures under operation conditions of hydrogen, oxygen, and water, respectively, normalized to 101 325 Pa.

Closely following the analysis given by Neyerlin *et al.*[28] (see also **Beginning-of-life MEA performance — Efficiency loss contributions**, Volume 3), the ORR overpotential can be given by equation (3)

$$\eta_{\text{ORR}} = \frac{2.3RT}{a_{\text{c}}F} \log\left[\frac{i}{10L_c A_{\text{Pt, ec}} i_{0,s}^{\text{eff}} \left(\frac{\text{p}_{\text{O}_2}}{\text{p}^*_{\text{O}_2}}\right)^{\gamma}}\right] \tag{3}$$

where $i_{0,\text{s}}^{\text{eff}}$ and γ are the effective exchange current density (normalized to the electrochemical platinum surface area) and the kinetic reaction order, and where L_{c} and $A_{\text{Pt, ec}}$ are the Pt loading (in mg Pt cm^{-2}) and the electrochemical active Pt surface area (in m^2 g^{-1} Pt), respectively. All other parameters have their usual meaning. Note that the pressure term is normalized to a standardized oxygen pressure of 101 325 Pa. The kinetic reaction order, γ, can be determined from experimental data using different oxygen partial pressures at constant temperature and oxygen overpotential according to equation (4):

$$\left.\frac{\partial \log i}{\partial \log \text{p}_{\text{O}_2}}\right|_{\eta_{\text{ORR}}, T} = \gamma \tag{4}$$

Finally, the activation energy can be determined at the reversible potential ($\eta_{\text{ORR}} = 0$) and constant oxygen partial pressure using the relationship in equation (5).

$$2.3\ \left.\frac{\partial \log i_{0,\text{s}}^{\text{eff}}}{\partial 1/T}\right|_{\eta_{\text{ORR}}=0, \text{p}_{\text{O}_2}} = -E_C^{\text{rev}} \tag{5}$$

Using experimental data sets for oxygen reduction at a temperature range from 120 °C to 160 °C and oxygen partial pressures from 20 to 200 kPa, all kinetic parameters can be determined by equations (3–5). Figure 5(b, c) illustrate the plots for determination of the reaction order and the activation energy; Table 2 summarizes the kinetic parameters of Celtec-P1000 cathodes in comparison to a low-temperature fuel cell cathode.[28]

From a detailed analysis of Table 2, it becomes clear that both the reaction order (0.52 ± 0.05 vs. 0.54 ± 0.02 for high and low temperature), activation energy (70 ± 2 kJ mol^{-1} vs. 67 ± 1 kJ mol^{-1} for high and low temperature), and the transfer coefficient are identical in a high-temperature cathode with a Pt/PBI/PA interface and a low-temperature cathode with a Pt/Nafion/water interface, respectively. It can be concluded that, in both cases, the ORR is following identical reaction mechanisms. This is an important finding that helps to understand performance differences between the two PBI and Nafion-type fuel cell cathodes. The only significant difference in the kinetic parameters can be found within the value of the exchange current densities. A direct comparison of its normalized values (80 °C, 101.3 kPa) reveals roughly 2.5 orders of magnitude higher value for the Nafion-type cathode, which explains the overall performance difference between high and low-temperature PEMFCs.

More relevant comparisons of the mass-specific and surface-specific current densities at 0.9 V, respectively, are also given in Table 2, whereas the values for the high-temperature fuel cell cathode closely mirrors typical activities observed in PAFC (with specific current densities at 0.9 V of 40–9 60 μA cm^{-2} Pt at 177 °C (see **Catalyst studies and coating technologies**, Volume 4), and approximately 20–50 mA mg Pt (see **Pt alloys as oxygen reduction catalysts**, Volume 3),[32] the activities in low-temperature fuel cell cathodes are typically in the range of 5–10 times higher at constant cell potential of 0.9 V, which is also found under more realistic conditions using H_2 air in the potential range of 0.7–0.8 V.[33] As discussed in this reference and also observed from Figure 4(a), due to the

Table 2. Comparison of cathode kinetic parameters of a Celtec-P1000 high-temperature cathode (Pt-PBI/phosphoric acid interface) and a low-temperature cathode (Pt-Nafion/water interface). Low-temperature data are taken from Neyerlin *et al.*[28] [Reproduced by permission of ECS – The Electrochemical Society.]

	PBI/H_3PO_4 interface Celtec-P1000	Nafion interface low-temperature PEFC
α_c	1	1
γ	0.52 ± 0.05	0.54 ± 0.02
E_{act} at $\eta_{ORR} = 0$ (from i_0^* at $p_{O_2} = 101.3\,kPa$)	$70 \pm 2\,kJ\,mol^{-1}$	$67 \pm 1\,kJ\,mol^{-1}$
i_0^* at $p_{O_2} = 101.3\,kPa$ and $T = 433\,K$	$4.3 \times 10^{-9}\,A\,cm^{-2}$ Pt	
i_0^* at $p_{O_2} = 101.3\,kPa$ and $T = 353\,K$	$5.2 \times 10^{-11}\,A\,cm^{-2}$ Pt (extrapolated)	$2.5 \times 10^{-8}\,A\,cm^{-2}$ Pt
i_m* ($A\,mg^{-1}$Pt) at 0.9 V, $p_{O_2} = 101.3\,kPa$	$0.017\,A\,mg^{-1}$ (433 K)	$0.13\,A\,mg^{-1}$ (353 K)
	$0.035\,A\,mg^{-1}$ (453 K)	
i at 0.9 V, $p_{O_2} = 101.3\,kPa$	$2.7 \times 10^{-5}\,A\,cm^{-2}$ Pt (433 K)	$2.5 \times 10^{-4}\,A\,cm^{-2}$ Pt (353 K)
	$6.0 \times 10^{-5}\,A\,cm^2$ Pt (453 K)	

differences in the Tafel slope in the different temperature regimes, lowering the cell potentials significantly increases the performance benefit of a low-temperature versus a high-temperature cathode.

Irrespective of the operation point at which low- and high-temperature cathodes are compared, it is important to understand the kinetic differences. The relationship in equation (6) can be used for deeper insights,

$$i_{0,s}^{eff}\left(\frac{p_{O_2}}{p_{O_2}^*}\right)^{\gamma} = i_{0,s}^*(1-\Theta)^x(c_{O_2}^0)^{\gamma} \qquad (6)$$

where the effective exchange current density (see equation 3) is replaced by the "real" exchange current density and a term describing the surface coverage by spectator species, $(1 - \Theta)$, with x being another reaction order describing the adsorption/desorption kinetics of respective spectator species. The pressure term in this relationship is formally substituted by the oxygen solubility, $c_{O_2}^0$ (applying Henry's law). Since it could be shown that in the low- and high-temperature cathode, the ORR follows identical reaction mechanisms for the same catalyst (Pt), it can follow that the "real" exchange current density is also identical and the observed overpotential differences are just determined by the number of free adsorption sites for the ORR to proceed (the $(1-\Theta)$-term) and the solubility of oxygen in the electrolyte. The number of free adsorption sites for the ORR in PA is limited due to the presence of relatively strongly adsorbing PA anions (dihydrogen phosphate and hydrogen phosphate) in large concentrations (note that under operating conditions the acid concentration is 90% and higher). Nafion, in turn, is basically a nonadsorbing electrolyte offering many more free reaction sites, and therefore a lower overpotential is observed. Secondly, the solubility of oxygen in PA is significantly decreased with temperature and acid concentration.[34] At temperatures below 60 °C, it was found that oxygen is enriched in Nafion compared to H_3PO_4, implying that the solubility of oxygen in Nafion is significantly larger than that of PA.[35] These findings suggest that part of the performance differences of high-temperature cathodes in a PBI/H_3PO_4 environment versus Nafion-type LT cathode can be related to limited oxygen solubility.

On the basis of the aforementioned analysis, it has to be concluded that significant performance improvements of cathodes operating in a PA electrolyte on Pt-based catalysts can only be achieved by finding a way to reduce adsorption of phosphate anions and/or by increasing the solubility of oxygen in the PA electrolyte. Indeed, several approaches have been undertaken in the past by using fluorinated electrolyte additives to influence the solubility term, but success has been limited thus far.[36, 37]

4.2 Membrane durability

MEA durability can be affected by the following typical membrane degradation modes: (i) the possibility of pinhole formation due to thinning of the membrane, which leads to increased fuel crossover and loss of fuel efficiency and (ii) acid evaporation. By choosing the appropriate gasket material, the former effect can be minimized even over extended operation times, e.g., the data on the 20 000-h test shown in Figure 3. Most importantly, hard gasket materials that do not deform at the applied pressure between the flow field plates at the operating temperature of an actual fuel cell are most suitable. Using these gaskets, the pressure on the MEA itself can be effectively reduced.

The latter effect, that is, acid evaporation due to the operating temperature range of 120–200 °C was found to be of no concern due to the unique properties of the membrane. Figure 6(a) illustrates the PA evaporation rates

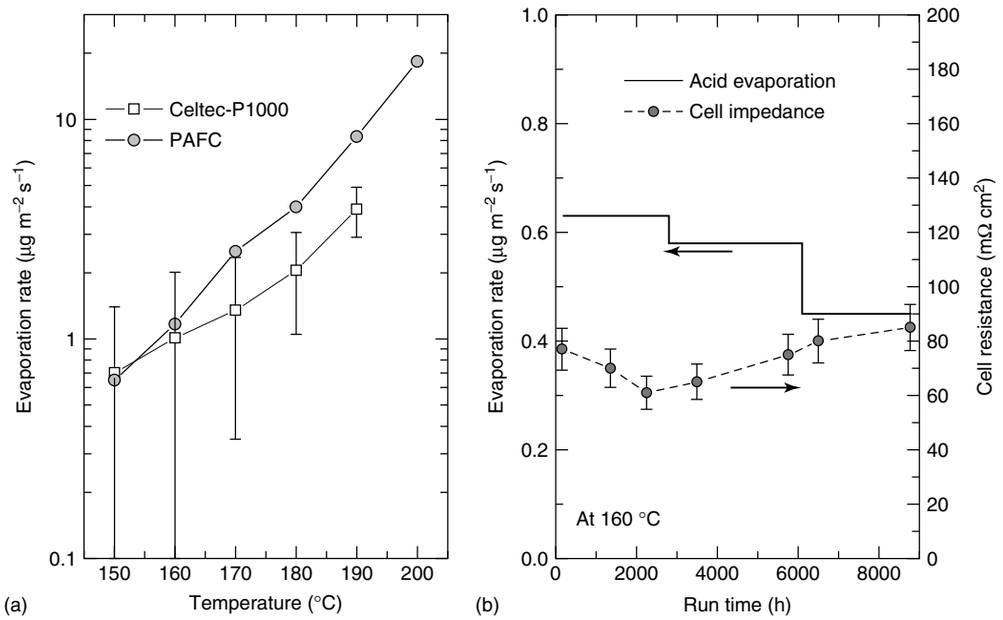

Figure 6. (a) Phosphoric acid evaporation rates in Celtec® MEAs at the beginning of life as function of temperature. For comparison, PAFC data from the literature are included. PAFC data are extracted from Okae and coworkers.[38] (b) Phosphoric acid evaporation rate in Celtec® MEA operated at 160 °C over a period of one year (left axis) and the cell resistances measured by 1-kHz AC impedance spectroscopy (right axis).

at the beginning of the life of Celtec® MEAs (determined in the first 100 h of operation) as a function of operating temperature. As a comparison, the evaporation data from a PA fuel cell system is plotted using the data in Ref. [38].

Typically, at the beginning of life, the measured acid evaporation rates are higher than those after longer operation since the MEAs are slowly approaching their equilibrium, and at first, some excess acid is evaporated. As shown in Figure 6(a), at the typical operating temperatures for the Celtec® MEAs of up to 180 °C, the maximum acid evaporation rate is around 2 $\mu g\,m^{-2}\,s^{-1}$ and only at higher temperatures do the rates increase significantly. However, as is quite obvious from Figure 6(a), the acid evaporation rates observed in Celtec MEAs are roughly a factor of 1.5–2 below the measured rates in a PA fuel cell, highlighting the unique chemical interaction between PBI membranes and PA, in contrast to the only physical interaction of the SiC matrix and PA in a PAFC.

In order to gather some experimental values of acid evaporation rates for longer MEA lifetimes, Figure 6(b) demonstrates the rates over a 1-year test at 160 °C for a Celtec®-P1000 MEA with approximately 100–200-μm membrane thickness. As illustrated, the acid evaporation rates decreased during the test (see above) and the overall value can be calculated to approximately 0.5 $\mu g\,m^{-2}\,s^{-1}$. In order to get precise numbers for the acid evaporation rates, we chose a rather long sampling time for the product water, and finally three samples were titrated to determine the acid content.

Given the amount of acid in the initial MEA, the experimentally determined acid evaporation rate, and defining the end of life of the MEA, as when 50% of the initial acid in the membrane is evaporated, a calculated lifetime of far more than 100 000 h can be reached. Another important value to describe MEA stability with respect to acid evaporation is the ohmic cell resistance, since reduced acid content in both the membrane (in terms of PA molecules/PBI repeat unit) and the catalyst layer will be increased. Also, due to the thinning effects of the membrane, an increase in contact resistance will be observed. In order to gain some insight, we measured the ohmic cell resistance over 8800 h of operation. The ohmic cell resistance changed by only $\pm 15\,m\Omega\,cm^2$, demonstrating that there is no significant impact of acid evaporation on cell lifetime.

4.3 Cathode stability

As known from the 1970s and 1980s, during the period of research and development of PAFCs, cathode durability is a critical factor for long-term fuel cell operation (see **Catalyst studies and coating technologies**, Volume 4). As several of our own studies have demonstrated, this is also valid for PBI-based MEAs.[19, 39] Although cathode degradation may not be severe for constant operation modes and for only several thousand hours of operation, longer operation times (over several ten thousand hours) require very stable cathodes. Additionally, very dynamic operation with many

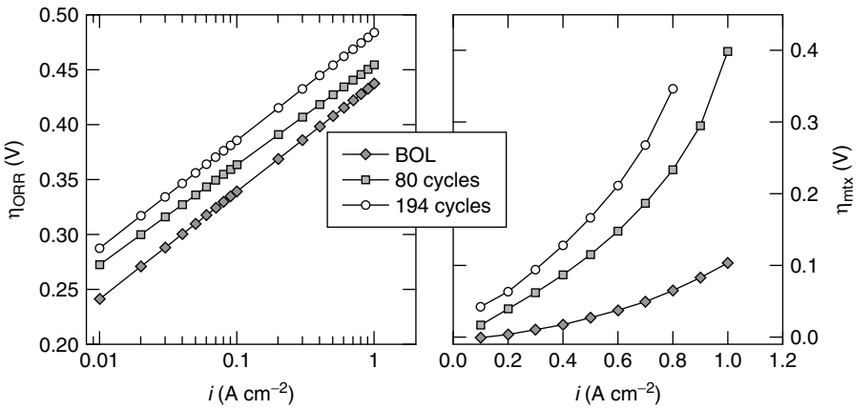

Figure 7. ORR and mass-transport overpotential development as function of cycle number in a voltage cycling test (cycling between 0.6 and 0.85 V, 180 °C) calculated as described in Ref. [39]. [Reproduced from Ref. [39] © Elsevier, 2008.]

voltage changes, such as changes to cell potentials above 0.75 V, e.g., in standby modes, start–stop operation, etc., typically leads to significantly higher cathode degradation as compared to constant load operation.

The typical electrode degradation modes are (i) corrosion of the catalyst metal (both particle growth and dissolution) (see **Catalyst and catalyst-support durability**, Volume 5), and (ii) corrosion of the carbon materials in electrodes (catalyst support and gas diffusion layer (GDL) materials) (see **Carbon-support corrosion mechanisms and models**; **Electrode degradation mechanisms studies by current distribution measurements**, Volume 6).

The two modes of electrode degradation stated above are both strong functions of the electrochemical potential and the operating temperature. Pt-metal particle growth can occur through Ostwald ripening in a simple surface diffusion process or through a dissolution/recrystallization process.[40] Pt dissolution concomitant with an irreversible loss of the active metal phase can become a severe issue when the fuel cell is operated for extended periods of time at potentials above 0.8 V (see **Stack materials and stack design**, Volume 4).[40] Both modes lead to the reduction of the electrochemical active surface area and manifest mainly as a decrease of the cathode kinetics. Both effects, especially carbon corrosion, are also triggered during start–stop operation where potentials above 1.3 V on the cathode were measured (see **Carbon-support corrosion mechanisms and models**, Volume 6).[41, 42] Therefore, it is of high importance to develop and study new catalysts and catalyst support materials. In what follows, we share some results from BASF Fuel Cell's development efforts for stabilizing the cathode. In order to study the stability of catalysts and catalyst supports toward corrosion, we performed a cathode voltage cycle test where the cathode potential is cycled between 0.6 and 0.85 V at 180 °C. This test probes both the stability of the catalyst metal and the support material, respectively. Figure 7 demonstrates the changes in both ORR and mass-transport overpotential when using a cathode with a Pt-alloy supported on Vulcan XC72 (30% Pt-Alloy#1/Vulcan, 1 mg cm^{-2} total metal cathode loading). As is obvious from Figure 7, the oxygen overpotential is increasing by almost 45 mV, almost 200 cycles, whereas the mass-transport overpotential in the cathode (e.g., at 0.8 A cm^{-2}) is increasing by almost 280 mV. Although it cannot be determined from this test alone if the kinetic changes are related to the loss of electrochemical surface area by particle growth, metal dissolution, or electrical disconnection of metal particles (all three effects likely play a role), these results clearly demonstrate that severe corrosion of the cathode catalyst takes place. The significant increase in mass-transport overpotentials clearly points to carbon corrosion effects leading to the flooding of the cathode catalyst layer.

Figure 8(a) illustrates a comparison of different cathode catalysts using the same voltage cycle test. For comparison, the voltage change at 0.8 A cm^{-2} measured in H_2–air polarization curves (stoichiometry 1.2/2) at 0.8 A cm^{-2} is plotted as a function of cycle number and catalyst type. In this comparison, we used the aforementioned Pt-alloy#1/Vulcan XC72, Pt-alloy#2/SC#1, and Pt-alloy#3/SC#2 (stabilized carbon). Figure 8 clearly reveals the stability of a newly developed Pt-alloy supported on a stabilized carbon in 300 V cycles with only minor decrease of cell potential at 0.8 A cm^{-2} (Note the initial increase in cell voltage is explained by slight improvements of catalyst utilization). This important development is the key for stabilizing the cathode for extended operation times of real-life fuel cell systems. However, one of the main tasks is not only providing cathodes with improved stability, but also provide cathodes, which show similar or better beginning of life performance than, e.g., cathodes with Vulcan-supported catalysts. Very often, the issue is increasing difficulties in processing and forming porous layers when working with highly corrosion-resistant carbons. Figure 8(b), however,

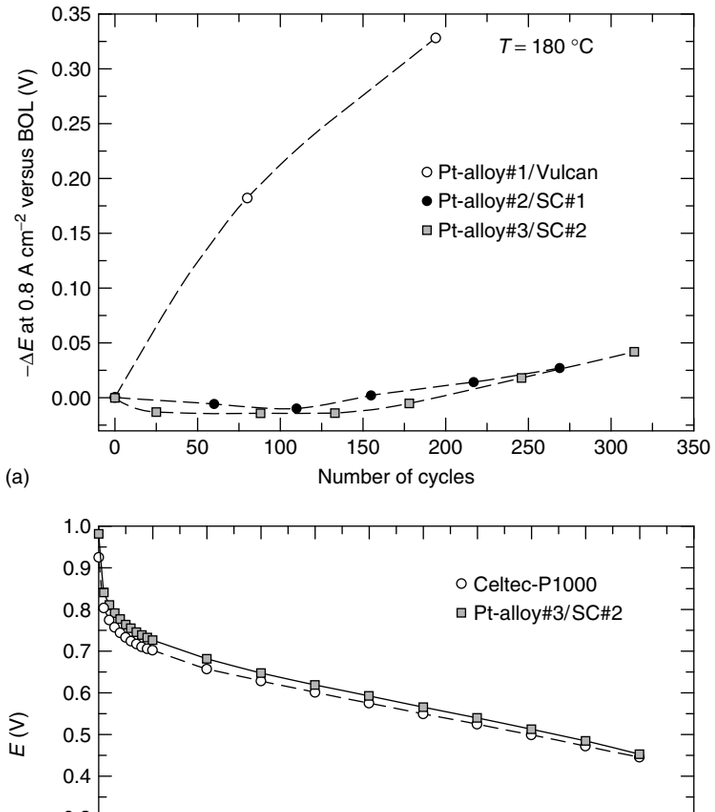

Figure 8. (a) Cell voltage difference at 0.8 A cm^2 versus BOL (*beginning of life*) in H_2 air (stoichiometry 1.2/2) operation at 180 °C for three different Pt-alloys using Vulcan XC72 (30 wt%) and two differently stabilized carbon (SC, 20 wt%) as function of the number of voltage cycles (0.85–0.6 V cycle). The cycles were performed using H_2–O_2 (stoichiometry 1.2/2) at 180 °C with 30 min holding time at each potential. Total cathode metal loading is 1 mg cm^{-2}. (b) Beginning of life polarization curve using H_2–air (stoichiometry 1.2/2) at 160 °C and 1 bar_a for a standard Celtec®-P1000 MEA and an MEA using a cathode with Pt-alloy#3/SC#2.

demonstrates the successful implementation of a corrosion-stable catalyst into a high-temperature MEA with even improved performance versus our Celtec®-P1000 MEA.

In summary, it has been demonstrated that the intrinsic stability against corrosion of the materials used in the cathode can be improved. Quite notably, the use of more stable catalyst supports is a major focus in order to improve the stability of an MEA. Besides the typical improvements to carbon itself (such as through graphitization[43]), other possibilities have to be considered, such as the adaptation of ceramics or other high-temperature, stable, electronically conductive materials like tungsten carbides or metal oxides. However, due to the difficulty of combined temperature stability with chemical and electrochemical stability in an acidic environment together with electronic conductivity, the materials science of support materials remains one of the most important topics in the research and development of fuel cells.

5 CONCLUSION

PBI is an excellent material for PA polymer electrolyte membranes. High-temperature operation allows for high CO tolerance, fast electrode kinetics, and simplified water and thermal management. When prepared by the PPA process, PBI shows improved mechanical properties, proton conductivities, and fuel cell operational characteristics compared to the conventionally prepared PBI-based membranes for high-temperature fuel cell applications. From

a commercial perspective, several fuel cell systems using Celtec® PBI-based MEAs are available in small scale with already proven long-term stability. It is, however, very important to continuously improve the lifetime of MEAs in fuel cell systems in order to reach the very long systems lifetimes that are required (>40 000 h for stationary applications).

REFERENCES

1. P. Jannasch, *Curr. Opin. Colloid. In.*, **8**, 96 (2003).
2. R. Savinell, E. Yeager, D. Tryk, U. Landau, J. Wainright, D. Weng, K. Lux, M. Litt and C. A. Rogers, *J. Electrochem. Soc.*, **141**, L46 (1994).
3. L. Xiao, H. Zhang, E. Scanlon, L. S. Ramanathan, E. -W. Choe, D. Rogers, T. Apple and B. C. Benicewicz, *Chem. Mater.*, **17**, 5328 (2005).
4. J. R. P. Jayakody, S. H. Chung, L. Duantino, H. Zhang, L. Xiao, B. C. Benicewicz and S. G. Greenbaum, *J. Electrochem. Soc.*, **154**(2), B242 (2007).
5. J. T. Wang, R. F. Savinell, J. Wainright, M. Litt and H. Yu, *Electrochim. Acta*, **41**, 193 (1996).
6. R. F. Savinell and M. H. Litt, 'Proton Conducting Polymer Electrolytes Prepared By Direct Acid Casting', WO Patent 9737396 (1997).
7. J. S. Wainright, R. F. Savinell and M. H. Litt, 'Proceedings of the International Symposium on New Materials for Fuel Cell and Modern Battery Systems, 2nd', Montreal, p. 808, 1997.
8. Q. Li, C. Pan, J. O. Jensen, P. Noyé and N. J. Bjerrum, *Chem. Mater.*, **19**, 350 (2007).
9. Q. Li, H. A. Hjuler and N. J. Bjerrum, *J. Appl. Electrochem.*, **31**, 773 (2001).
10. D. Mecerreyes, H. Grande, O. Miguel, E. Ochoteco, R. Marcilla and I. Cantero, *Chem. Mater.*, **16**(4), 604 (2004).
11. L. Xiao, H. Zhang, T. Jana, E. Scanlon, R. Chen, E. -W. Choe, L. S. Ramanathan, S. Yu and B. C. Benicewicz, *Fuel Cells*, **5**, 287 (2005).
12. E. Scanlon, *Prepr. Pap.-Am. Chem. Soc., Div. Fuel Chem.*, **49**(2), 522 (2004).
13. R. D. Breault, 'Silicon Carbide Electrolyte Retaining Matrix for Fuel Cells', US Patent 4017664 (1970).
14. W. Spearin, 'Process for Forming a Fuel Cell Matrix', European Patent EP 0344089 (1989).
15. R. D. Breault, 'Silicon Carbide Electrolyte Retaining Matrix for Fuel Cells', US Patent 40117664 (1977).
16. S. Haile, D. A. Boysen, C. R. I. Chisholm and R. B. Merle, *Nature*, **410**, 910 (2001).
17. T. Uda and S. Haile, *Electrochem. Solid Lett.*, **8**, A245 (2005).
18. K. D. Kreuer, *ChemPhysChem.*, **3**, 771 (2002).
19. T. J. Schmidt, *ECS Trans.*, **1**(8), 19 (2006).
20. T. J. Schmidt and J. Baurmeister, *ECS Trans.*, **3**(1), 861 (2006).
21. J. N. Allen, N. Sifer and E. Bostic, 'The XX25: A 25W Portable Fuel Cell for Soldier Power', "Proceedings of the 42nd Power Sources Conference", Philadelphia, PA, p. 403, 2006.
22. L. Gubler, D. Kramer, J. Belack, Ö. Ünsal, T. J. Schmidt and G. G. Scherer, *J. Electrochem. Soc.*, **154**, B981 (2007).
23. K. A. Perry, G. A. Eismann and B. C. Benicewicz, *J. Power Sources*, **177**, 478 (2008).
24. R. Makharia, S. Kocha, P. Yu, M. A. Sweikart, W. Gu, F. Wagner and H. A. Gasteiger, *ECS Trans.*, **1**(8), 3 (2006).
25. T. D. Jarvi, H. A. Gasteiger and S. Cleghorn (Eds), 'Durability and Reliability of Proton Exchange Membrane Fuel Cell', "ECS Transactions", The Electrochemical Society, Pennington, NJ, Vol. 1(8) (2006).
26. T. Fuller, T. V. Nguyen, T. D. Jarvi, V. Ramani, E. M. Stuve, C. Bock, M. F. Mathias, H. A. Gasteiger, S. Cleghorn and T. Zawodzinski (Eds), 'Proton Exchange Membrane Fuel Cells 6', "ECS Transactions", The Electrochemical Society, Pennington, NJ, Vol. 3(1), (2006).
27. F. N. Buechi, M. Inaba and T. J. Schmidt (Eds), 'Durability and Degradation of PEFCs', Springer, New York.
28. K. C. Neyerlin, W. Gu, J. Jorne and H. A. Gasteiger, *J. Electrochem. Soc.*, **153**, A1955 (2006).
29. H. R. Kunz and G. A. Gruver, *Electrochim. Acta*, **23**, 219 (1978).
30. K. C. Neyerlin, W. Gu, J. Jorne and H. A. Gasteiger, *J. Electrochem. Soc.*, **154**, B631 (2007).
31. D. R. Lide, 'CRC Handbook of Chemistry and Physics', CRC Press, Boca Raton, FL (1995).
32. K. Kinoshita, 'Electrochemical Oxygen Technology', John Wiley & Sons, New York. (1992).
33. H. A. Gasteiger and J. Garche, 'Fuel Cells', in "Handbook of Heterogeneous Catalysis", G. Ertl, H. Knözinger, F. Schüth and J. Weitkamp (Eds), Wiley-VCH, Weinheim, p. 3081 (2008).
34. K. E. Gubbins and R. D. Walker Jr., *J. Electrochem. Soc.*, **112**, 469 (1965).
35. S. Gottesfeld, I. D. Raistrick and S. Srinivasan, *J. Electrochem. Soc.*, **134**, 1455 (1987).
36. M. Razaq, A. Razaq, E. Yeager, D. D. DesMarteau and S. Singh, *J. Electrochem. Soc.*, **136**, 385 (1989).
37. D. J. Burton, 'Synthesis of Novel Fluorinated Phosphonic Acid Electrolytes for Phosphoric Acid Fuel Cells', Final Report, Contract No. 5084-260-1081, Gas Research Institute (1992).
38. I. Okae, S. Kato, A. Seya and T. Kamoshita, 'Study of the Phosphoric Acid Management in PAFCs', "The Chemical Society of Japan 67th Spring Meeting", p. 148, 1990.
39. T. J. Schmidt and J. Baurmeister, *J. Power Sources*, **176**, 428 (2008).
40. P. N. Ross Jr, 'Deactivation and Poisoning of Fuel Cell Catalysts', in "Catalyst Deactivation", E. E. Petersen and A. T. Bell (Ed.), Marcel Dekker, New York, p. 167 (1987).
41. C. A. Reiser, L. J. Bregoli, T. W. Patterson, J. S. Yi, J. D. Yang and M. L. Perry, *Electrochem. Solid-State Lett.*, **8**(6), A273 (2005).
42. T. J. Schmidt, 'High-Temperature PEFC: Durability Insights', in "Durability and Degradation of PEFCs", F. N. Buechi, M. Inaba and T. J. Schmidt (Ed.), Springer, in press.
43. K. Kinoshita, 'Carbon Electrochemical and Physicochemical Properties', John Wiley & Sons, New York (1988).